The far-infrared spectroscopic surveyor (FIRSS)

Experimental Astronomy
https://doi.org/10.1007/s10686-021-09716-w

ORIGINAL ARTICLE

The far-infrared spectroscopic surveyor (FIRSS)

D. Rigopoulou[1] · C. Pearson[2] · B. Ellison[2] · M. Wiedner[3] · V. Ossenkopf Okada[4] · B. K. Tan[1] · I. Garcia-Bernete[1] · M. Gerin[3] · G. Yassin[1] · E. Caux[5] · S. Molinari[6] · J. R. Goicoechea[7] · G. Savini[8] · L. K. Hunt[9] · D. C. Lis[10] · P. F. Goldsmith[10] · S. Aalto[11] · G. Magdis[12] · C. Kramer[13]

Received: 3 August 2020 / Accepted: 2 March 2021 / Published online: 26 May 2021

Abstract

We are standing at the crossroads of powerful new facilities emerging in the next decade on the ground and in space like ELT, SKA, JWST, and Athena. Turning the narrative of the star formation potential of galaxies into a quantitative theory will provide answers to many outstanding questions in astrophysics, from the formation of planets to the evolution of galaxies and the origin of heavy elements. To achieve this goal, there is an urgent need for a dedicated space-borne, far-infrared spectroscopic facility capable of delivering, for the first time, large scale, high spectral resolution (velocity resolved) multiwavelength studies of the chemistry and dynamics of the ISM of our own Milky Way and nearby galaxies. The Far Infrared Spectroscopic Surveyor (FIRSS) fulfills these requirements and by exploiting the legacy of recent photometric surveys it seizes the opportunity to shed light on the fundamental building processes of our Universe.

Keywords ISM: Galaxies · Space Vehicles: Instruments · Techniques: Spectroscopy · ESA Voyage2050

1 Introduction

The far-infrared (FIR) to submillimetre (sub-mm) window is one of the least-studied regions of the electromagnetic spectrum. Yet, this wavelength range is absolutely crucial to our understanding of star formation and galaxy evolution in the Universe. The complex processes that convert gas into stars leave their imprint on the interstellar medium (ISM) of the Galaxy and external galaxies (Fig. 1). FIR continuum emission has been widely used as a mass tracer of the ISM. This continuum emission is

✉ D. Rigopoulou
dimitra.rigopoulou@physics.ox.ac.uk

Extended author information available on the last page of the article.

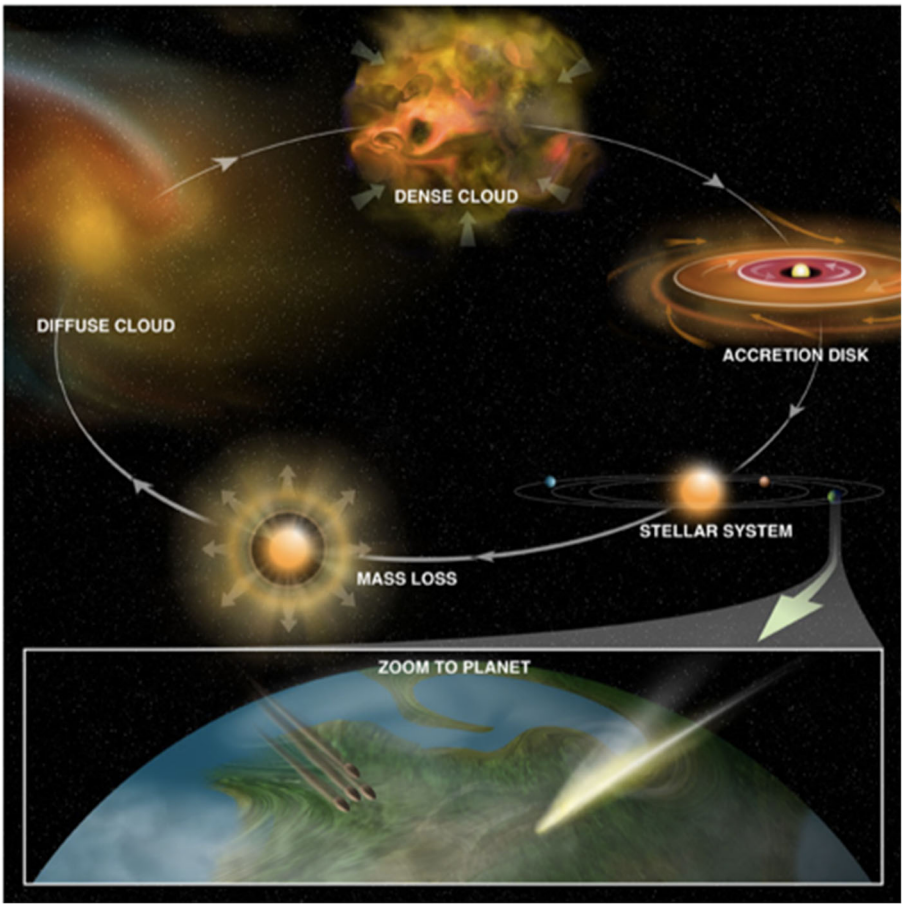

Fig. 1 The cycle of gas and dust in galaxies: from interstellar clouds to stars and planets (credit: Bill Saxton, NRAO/AUI/NSF)

the result of the integrated contribution of the different ISM components distributed along the line-of-sight (LOS). Therefore, it is impossible to use this integrated emission to isolate and study the various ISM components separately. Fortunately, the FIR regime is also rich in atomic, ionized, and molecular spectral lines, which can be detected and characterized via high-resolution spectroscopy.

Previous IR missions (IRAS, ISO, Spitzer, AKARI, Herschel, and Planck) have made great strides in elucidating the properties of the coldest and densest components of the ISM and, the mechanisms that lead to the formation of stars and planets, the building blocks of galaxies. However, all of these missions have had limited ability to fully probe the ISM and especially its velocity structure which is key to unlocking its properties. The fine-structure line of singly ionised carbon [CII] at 158 μm is the most important cooling line of the neutral ISM and is the brightest line in the spectrum of the Milky Way and many external galaxies. Together with the singly ionized

nitrogen line [NII] at 205 μm it can be used to measure the amounts of gas in different phases of the ISM, from ionized to atomic/neutral. The 63 μm and 145 μm fine structure lines of neutral oxygen [OI] are excellent probes of the conditions in regions surrounding newly-formed massive stars and is thus a measure of the feedback from these stars that helps regulate the rate of star formation. Carbon, Oxygen, and Nitrogen are the most abundant elements in the Universe after Hydrogen and Helium. They are found everywhere: from the first massive stars that formed and died long ago to the Carbon in our body and the Oxygen we breathe.

The FIRAS/COBE instrument [7] spectroscopically surveyed the whole sky from 0.1 mm to 10 mm with a spatial resolution of 7° and a velocity resolution of 1000 km/sec. FIRAS determined that the [CII] line is the dominant cooling line of the ISM at 0.3% of the continuum infrared emission while the [NII] and CI lines are less intense by a factor of 10 and 100, respectively. As reported by [28], all three lines peak in the central regions of our galaxy (the molecular ring) and originate from a layer with a thickness of a few degrees but the mission had insufficient spatial resolution to relate the emission to specific components and sources within the ISM. FIRAS/COBE was instrumental in determining the global characteristics of these atomic line tracers and brought the key questions that FIRSS will address to the forefront of ISM studies.

2 Science motivation

The interaction between stellar radiation and interstellar matter results in strong emission in the FIR to sub-mm wavelength range. Herschel's superb photometric capabilities afforded panoramic views of large areas of the Galaxy e.g. [69, 104] and deep regions of the extragalactic sky (e.g. [66, 78]). But these deep FIR images of dust emission provide 'static' snapshots of the complex processes that transform gas into stars. Without velocity resolved information it is impossible to fully understand the complex physics of the ISM and unravel the processes that turn gas into stars through cosmic time. The Far Infrared Spectroscopic Surveyor (FIRSS) mission aims to probe the multi-phase ISM by pursuing large-scale velocity resolved (3D) maps of key bright spectral lines (the dominant gas coolants) in our Galaxy, nearby and distant galaxies. FIRSS will carry out a wide area high spectral resolution (3D) survey of the infrared sky in four discrete spectroscopic bands: [CII] 158 μm, [NII] 205 μm, [CI] 390 μm, and [OI] 63 μm. The four FIRSS channels target fine structure (FS) lines that are fundamental probes of the physical conditions of the ISM. The [NII] and [CII] lines have very similar excitation conditions with critical densities around 100 cm^{-3} and upper level temperatures of 70K and 91K, respectively, so that simultaneous observations of both lines allow subtraction of the contribution of the ionized medium to the [CII] emission. Neutral atomic carbon occurs mainly in molecular gas where UV photons with more than 11.1 eV dissociate CO. Atomic oxygen [OI] traces all phases of neutral gas, including material with abundant CO, but has a high critical density of 5×10^5 cm^{-3} and upper level energy of 230 K, so strongly favours the warm dense gas in emission, while it can be traced from all other phases in

absorption in case of a sufficient background radiation level. In what follows we present the key FIRSS Science Objectives.

2.1 Galactic science

2.1.1 Phase structure of the ISM in the galaxy

The ISM gas in our Galaxy and external galaxies can be found in atomic, ionized or molecular state, with a range of densities and temperatures. The ISM can be further characterized by a few 'phases' depending on physical conditions: ionized gas is found as coronal gas in the hot ionized medium (HIM, at T$\sim 10^6$ K and n$\sim$ 0.04 cm^{-3}) and as warm ionized medium (WIM, at T$\sim 10^4$ K gas) in which most of the hydrogen is in H^+, and includes diffuse intercloud gas (with n$\sim$0.3 cm^{-3}) and denser HII regions (with n$\sim 10^4$ cm^{-3}) photoionized by nearby massive stars. In addition, two neutral atomic phases coexist at roughly thermal pressure equilibrium (e.g. [127]); the warm neutral medium (WNM, with T$\sim 10^4$ K and n$\sim$0.3 cm^{-3}) and the cold neutral medium (CNM, T$\sim$80 K and n$\sim$40 cm^{-3}). In the densest gas regions, hydrogen turns molecular, forming giant molecular clouds that are prime sites for star formation. However, in recent years, it has become apparent that the traditional distinction of the ISM into these well-separated, thermally and chemically stable phases does not reflect the dynamic nature of the ISM evolution. A large fraction of the gas can be found in transitional regions. To obtain a full inventory of the interstellar gas, observations of all phases and the transitions between them are needed. Local and global thermal pressure variations regulate the amount of material in the different phases. Pressure disturbances from shocks of expanding shells and spiral density waves can redistribute material from the WNM regime to the CNM component, where it is generally assumed that molecular gas develops. The pressure modulates the CNM/ WNM ratio and in turn, the molecular gas fraction [24]. Together with the tight correlation between molecular gas and the star-formation rate on galaxy scales this suggests that the gas pressure is a dominant parameter for star-formation. However, [55] have shown that these relations break down on the scale of giant molecular clouds and the observations in the central region of the Milky Way reveals low star-formation activity at high pressure [53]. To understand galactic star formation and the evolution of our Galaxy we need to measure the pressure and decompose it into thermal, turbulent, and magnetic components. This requires imaging of spectral line emission from well-defined tracers of the ionized, neutral atomic, and molecular gas phases of the ISM. The spectral maps measure the distribution of gas and establish spatial and kinematic relationships between different phases.

To follow the sequence of the formation of molecular clouds, dense clumps, and finally stars within them, we have to start by tracing the transition from atomic to molecular material, not only as a chemical transition, but also in terms of the velocity perturbations injected into the molecular clouds that in turn, create the density enhancements providing the seeds of star formation. Conventionally, the WNM and CNM phases are spectroscopically probed with the HI 21 cm line. However, the HI 21 cm line in emission cannot distinguish between WNM and CNM as it cannot reliably trace the spatial and kinematic boundary to the denser, molecular gas component.

The CNM is more directly studied through HI 21 cm absorption profiles towards background continuum sources but such sources with sufficient brightness are sparse precluding the construction of even a moderate resolution map of a CNM cloud and an evaluation of its key physical properties. The molecular gas can be examined with various molecular lines that trace different density regimes. The millimetre and sub-millimetre rotational lines of CO are the primary spectral line tracer of the molecular hydrogen in galaxies. However, CO is not sensitive to the regime where hydrogen is mostly molecular but the CO abundance remains very low due to photodissociation. This CO-dark H_2 gas may comprise a significant fraction (20-80%) of the molecular mass of galaxies [36, 89] and is best studied through the fine structure transition of ionized carbon (see below). Accurate estimates of the thermal pressure require velocity-resolved observations. To distinguish ionized and neutral gas a resolution of 2 km/s is sufficient, but to study the boundaries between the regions a resolution better than 1 km/s is required [22].

2.1.2 CO-dark gas: Measuring the real amount of ISM

Cold H_2 is not directly observable due to lack of electric dipole moment, resulting in the existence of the so-called dark molecular gas [35]. At depths where UV photons with energies above 11.2 eV can penetrate, carbon is ionized so that the gas emits [CII]. Deeper into the cloud there is a layer with a large fraction of atomic carbon visible in [CI] surrounding the "traditional molecular cloud" observable in CO. In both layers oxygen is atomic, but bright [OI] emission is only expected from dense gas ($n > 10^5 cm^{-3}$). Within the Galactic midplane, the Herschel GOTC$^+$ project provided a first measurement of the fraction of CO-dark molecular gas [56–58, 87, 89]. They found fractions between 20% and 75%. Similar analysis for individual star forming regions or regions with HI self-absorption also showed large fractions of CO-dark molecular gas ([74, 84, 111], see Fig. 2).

Following the fraction across the boundary of the Taurus cloud, [128] found values around 80% for visual extinctions below unity. So far, most studies have been conducted towards the dense region of the Galactic midplane. As the fraction of diffuse molecular material (or CNM) is higher in the plane compared to higher Galactic latitudes we expect that the fraction of CO-dark molecular gas is higher there. As a consequence, it is likely that currently we are severely underestimating the gas mass of the Milky Way. A high spectral resolution FIR mission such as FIRSS is the only way to reliably account for the missing gas. Tracing this gas is only possible by decomposing all phases of the ISM. For this we need to combine observations of a variety of ionized, atomic and molecular species ([NII], [CII], [CI], [HI], and CO).

Herschel and SOFIA observations have shown that far-IR fine structure lines of [CII], [OI], and [CI] can serve as spectroscopic tracers of neutral gas. The [CII] 158μm line arises in multiple environments with varying emissivity: from regions of ionized gas, the WNM and CNM, CO-dark H_2 gas, and photodissociation regions (PDR). To decompose the emission into each type of region, velocity-resolved measurements of the [CII] emission are necessary to compare with similarly velocity-resolved line profiles of CO and HI 21 cm line emission [88]. Any [CII] not associated with ionized gas, HI 21cm, and CO emission is assigned to the CO-dark

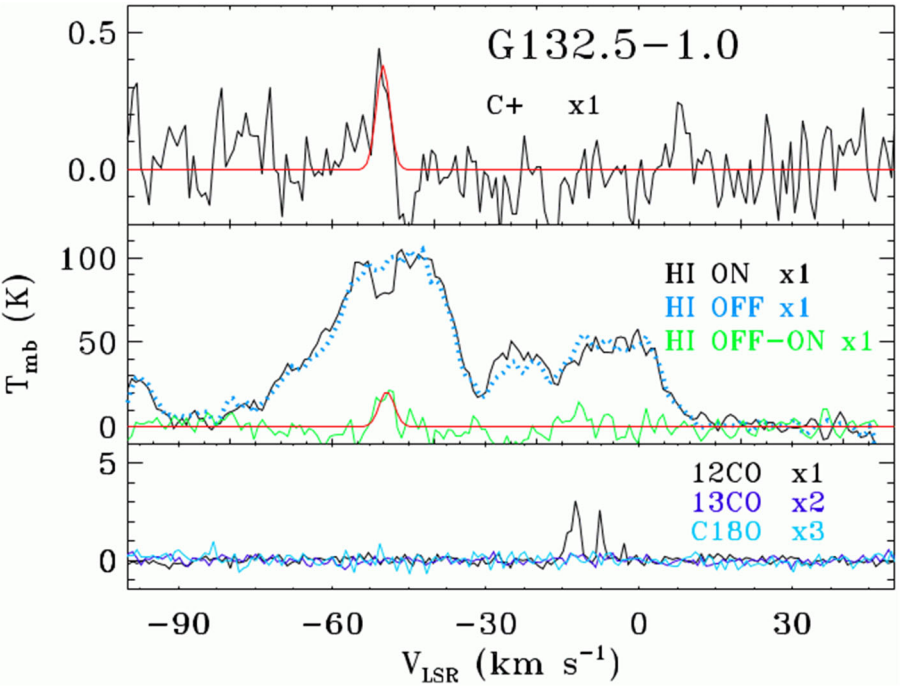

Fig. 2 Observations of different gas phases towards G132.5 [111]. Multiple components of warm neutral gas create very broad lines of HI emission. A narrow HI absorption feature stems from colder (presumably denser) neutral gas also detected in [CII] emission CO emission from dense molecular gas is only seen in a completely different velocity component

H_2 regime. A fraction of the CO-dark H_2 gas may also be visible in the fine structure lines of atomic carbon. The [OI] 63μm line is a strong coolant in denser (3000 cm^{-3}) regions but is optically thick under most conditions. The [OI] 145μm line is optically thin providing an important tracer of mass and column density in the dense PDR regions if sufficiently high temperatures are reached. Recent synthetic [CII] emission studies on the scales of Giant Molecular Clouds (GMCs) show its potential as the most straightforward tracer of the physical properties of the CO-dark gas and even the total gas of the cloud [6, 30, 107]. [CII] emission in these simulations coherently extends beyond the CO and [CI] emission. This requires velocity-resolved line profiles of [CII] emission, which can also define the kinematic relationships between various neutral gas phases that are predicted by spiral density wave theory [21, 98, 99]. The large scale distribution of the CO 1-0 and 2-1 lines [76, 90] showed a low typical CO 2-1/CO 1-0 ratio ~ 0.5 that can only be explained by excitation temperatures well below the kinetic temperature of the gas, indicating gas densities below the critical density of about 1000 cm^{-3}. In such gas, the CO self-shielding is usually not strong enough to prevent dissociation over long time scales, i.e. most gas will be in a transitional phase with [CII] observations required to trace this material.

Measuring the fraction of the CO-dark molecular gas as a significant fraction of the baryonic matter in our Galaxy is crucial as it is likely to lead to a paradigm shift in our understanding of the molecular gas reservoir of galaxies.

2.1.3 Feeding the Milky Way and its sites of star formation

GMCs are the exclusive sites of massive star and stellar cluster formation. The assembly and destruction of such massive ($M > 10^5\ M_\odot$) structures are critical steps in the star formation process and impact the gas depletion time that is encapsulated in the Kennicutt-Schmidt scaling relationship. Theoretical studies [33] have suggested that molecular clouds are formed by large-scale accretion of new material onto existing dense clouds. Their findings are consistent with observations that suggest the global filamentary structure of molecular clouds is created by large scale flows of atomic material at earlier times [69, 83, 124]. Gravity is an essential component of cloud formation as it facilitates the accumulation of gas over large scales. Perturbations to the local gravitational potential conducive to cloud formation are generated by spiral density waves, the interface of large-scale ($\sim 10^2$ pc) converging flows, and shells of interstellar material swept up by feedback processes. Nonetheless, mass accretion has not been convincingly demonstrated observationally. The material may either be accreted as atomic hydrogen or low-density molecular hydrogen. Atomic gas can be measured through the 21 cm atomic hydrogen line, but the emission is always highly confused by the warm neutral medium along the line of sight. Without the ability to separate the different ISM components, proper assessment of the atomic hydrogen emission is impossible. Molecular hydrogen is not detectable at low gas temperatures in the ISM and CO forms well after the H_2 column density is $>$ few $\times\ 10^{21}$ cm^{-2}, implying that the initial phases of the cloud formation process take place in the 'CO-dark' molecular gas. Goicoechea et al. [32] and Pabst et al. [81] directly observed the atomic 'Veil' of Orion, an expanding bubble created by the strong winds of young massive stars, in the largest ever velocity-resolved [CII] map, as shown in Fig. 3 for the innermost part of the map.

On smaller scales, infall through spurs has been observed in molecular lines [105]. To trace the accretion of material onto filaments and its effect on their structure and subsequent evolution, requires mapping surveys with reasonable angular resolution ($<$ 1 arcmin) together with large spatial coverage, with adequate velocity resolution to detect the predicted velocity shifts of less than or equal to 1 km/s. Only by detailed imaging of a significant sample of those filaments along with their dense cores and associated young stars, can we unravel the physics controlling the evolution of these structures and their role in the process of star formation.

Over the lifetime of the Galaxy, significant amounts of interstellar matter are ejected from the Galactic plane through the interaction of supernova explosions with their environment. This creates Galactic fountains [9] visible e.g. as Fermi Bubbles. They contain a significant amount of interstellar material but it is unclear to what degree the gas can leave the Galactic potential. A large fraction of the material falls back onto the Milky Way plane, often seen in terms of high-velocity clouds. Additional material is accreted by the Milky Way from the intergalactic gas and the

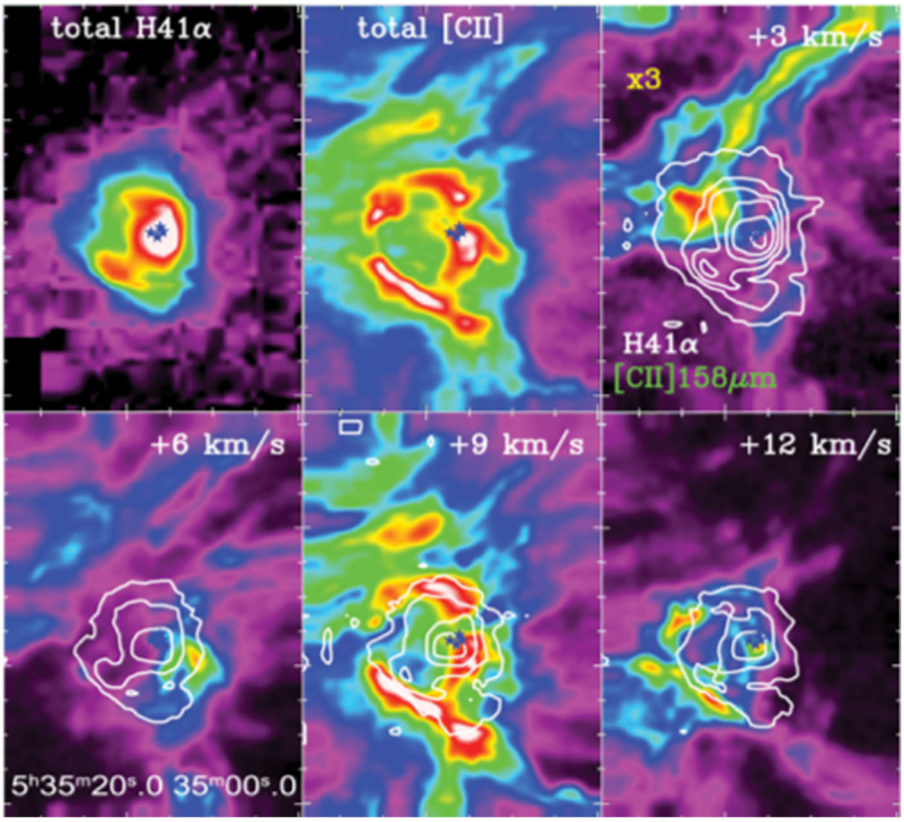

Fig. 3 [CII] map towards Orion measured in different velocity channels in comparison to the distribution of ionized gas. At v = 3km/s a stream of CO-dark molecular gas is visible [32]

neighbouring galaxies, e.g. through the Magellanic stream, but the relative importance of the different sources of material for feeding the Galactic ISM, the time scales, velocities, and dynamic impact on the turbulent velocity structure of the ISM are still completely unknown today. We have episodic evidence for this infall through observations of High-Velocity and Intermediate-Velocity Clouds (HVCs, IVCs, e.g. [122]), but no complete inventory that would provide a global picture. Due to their low density, a major fraction of the HVC and IVC gas is only traceable in the atomic fine-structure lines. In the Draco Cloud, produced by the collision of high-velocity material with Galactic ISM, only a small fraction of the total gas can be traced through HI and CO ([40, 82] (see also [68] for SPIRE imaging and more recent analysis in the context of colliding flows). To quantify the feeding of the Galactic ISM by molecular, atomic, and ionized gas and distinguish the different sources of this feeding a FIR fine structure line survey of the material above and below the Galactic plane is necessary.

2.1.4 Turbulent energy injection

Closely related to the cloud assembly is the question of how clouds acquire high levels of internal turbulence from the large-scale diffuse ISM. Statistical studies of GMCs have shown that clouds have highly non-thermal motions [43] and the main physical process that drives such supersonic motions operates on size scales comparable to or larger than the GMCs themselves [10]. Since turbulence is expected to decay over roughly a crossing time, it is puzzling how such intermittent sources of energy in the ISM can sustain the observed supersonic turbulence. Various solutions have been proposed that range from multi-scale gravitational collapse over Galactic shear to internally-driven (via stellar feedback) turbulence (see [21]).

Any accretion of gas by the Milky Way will create cloud collisions, typically described as "colliding flows", and they unavoidably create large-scale turbulent motions in the ISM. They could be responsible for a major fraction of the Milky Way ISM turbulence but the accretion contribution relative to the Galactic shear or supernova bubbles is still unknown. Using numerical models [50] find that in the Milky Way, the observed level of turbulence in the interstellar medium can be sustained by accretion, provided that the Galaxy gains mass at a rate comparable to that derived from its star-formation rate. To confirm this scenario, we need to obtain large scale statistics of clouds at high velocities, measuring the infall rate and the Mach number of the turbulent driving by accretion. Although the Galactic rotation curve and the spiral structure of the Milky Way are reasonably well known [114] the impact of Galactic shear on the driving of interstellar turbulence is still not clear because this requires information on the spiral arm gas, the interarm gas, and their interaction. Resolving the mutual velocities of the different ISM components measures the feeding of spiral arm gas in terms of mass and momentum. For a limited field, [118] have used HIFI [CII] observations to trace the contributions of different gas components to the spiral arm and interarm gas, resolving the internal structure of the spiral arms and measuring the compression of the warm-ionized medium induced by the spiral density waves. A global study for the interarm gas is still missing. This prevents us so far from computing the impact of Galactic shear on the structure of molecular clouds in the spiral arms.

Simulations of the impact of supernova explosions on the Galactic disc structure [29, 31] show that the relation between the scale height of the distribution of CO, atomic Carbon, and [CII] is very sensitive to the frequency and location of supernovae in the Milky Way. Supernova clustering and the impact of stellar winds before the supernovae produce a significant difference. By measuring the distribution of the scale heights of the [CI] and [CII] emission and comparing it with the known distribution of CO [15], we would be able to constrain these models and resolve local variations in the supernova driving in the last 100 Myr.

Distinguishing between these three scenarios requires a simultaneous study of the clouds and their diffuse environment to measure the flows and turbulence injection generated from accretion and feedback [116]. To do this demands detailed mapping with a tracer such as [CII] of the overall mass reservoir of the cloud and the diffuse ISM around it to determine velocities and their degree of spatial correlation with varying displacements. The [CII] emission maps obtained with Herschel and now

with SOFIA, limited in sensitivity and mapping area, are insufficient to address the issue of gas flows and turbulence. Large scale mapping of [CII] (several 10 pc) at high spectral resolution ($<<$ 1 km/s) is thus required to understand this aspect of GMC formation and evolution.

2.1.5 Stellar feedback

Radiative feedback from high-mass stars in dense clusters regulates the dynamics, thermal balance, and chemistry of the ISM. It is a multi-scale process influencing the star-forming regions in our own Galaxy and those in starburst galaxies locally and all the way to the early Universe. The [CII] emission from bright PDRs is one of the best tracers of massive, deeply embedded star formation ([32], Fig. 4). Since [CII] is mainly produced and excited from FUV radiation from massive stars, primarily from B stars that are relatively short-lived, the [CII] line appears as a natural tracer of the star-formation that occurred in the last 10 Myr. A strong correlation between the line intensity and the star-formation rate in galactic and extragalactic sources has long been noted (see e.g. [17, 42, 94]).

However, it has been found that the most luminous IR galaxies deviate strongly from this linear relation, showing a fine-structure-line deficit (e.g. [27]). The explanation for this behaviour remains unclear. However, a combination of high optical depths, foreground absorption, and regions of exceptionally large total column densities may be responsible. Crucially, the '[CII] deficit' is also seen in Orion, if one

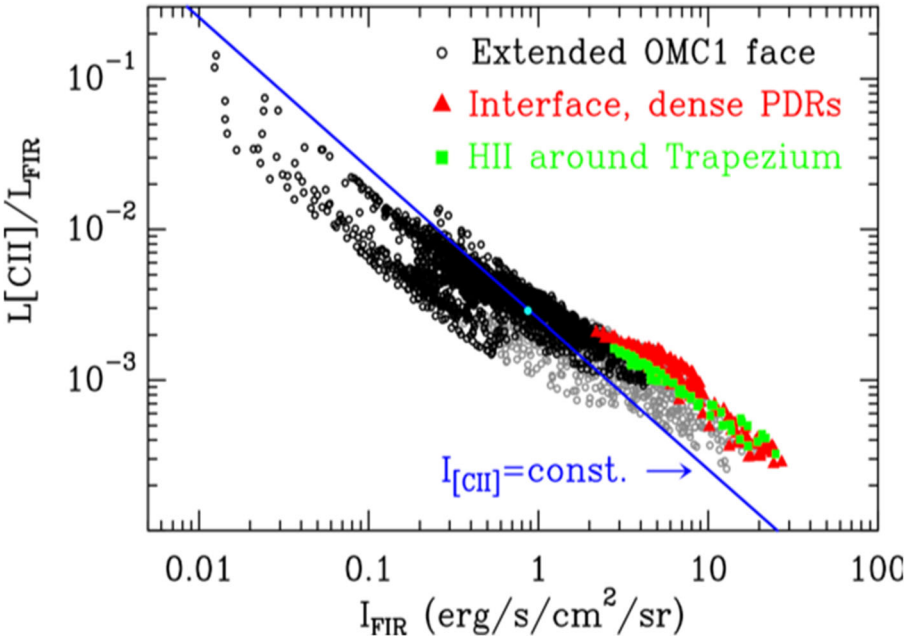

Fig. 4 [CII]/FIR luminosity ratio variation as a function of position in Orion [32]. This behavior is reminiscent of the "[CII] /FIR deficit" seen in local ULIRGs

examines the ratio between fine structure line and total infrared emission ([CII]/TIR ratio) as a function of dust opacity [32]. This may reflect the simple fact that the dust throughout the cloud all emits in the IR, but the [CII] emission is confined to the layer with Av <2 - 3 mag. Thus, the emitting regions in ULIRGs may well have 'dust emission excess' rather than a [CII] deficit.

Additional insight to this puzzle has been provided by velocity resolved [CII] observations with GREAT/ SOFIA. These observations showed that foreground absorption may be blocking part of the line profile ([60, 125], see Fig. 5). An estimate of the isotropically radiated power in the [CII] line is only possible if the unattenuated line profile can be fitted. In the extreme example of S140, [79] found that self-absorption can explain a line deficit of more than a factor 10 and showed that complementary observations of the [OI] line provide a key to estimate the foreground impact. In all cases it is necessary to use the velocity information from the [CII] line profiles to distinguish between the [CII] flux originating from the diffuse ISM and the material that is actually heated by young stars, i.e. can in principle trace the star formation rate [102]. It turns out that even in a massive star-forming region such as OMC1, only a minor fraction of the [CII] intensity traces the dense, star-forming gas while most of the [CII] emission is produced by an extended cloud face with a basically constant [CII] column density unaffected by the star-forming process. Measuring the actual fine-structure line cooling in the Milky Way through such velocity-resolved spectra will provide the final step for calibrating the [CII]-intensity to star-formation-rate ratio in the Milky Way which can then be applied to other galaxies near and far.

If spectrally resolved, the [CII] line can also measure the dynamics of radiative feedback in terms of the expansion velocity of HII regions and associated shells [81, 86]. However, for inhomogeneous, clumpy structures, the effective kinetic energy input through the different feedback processes (protostellar outflows, radiation pressure, photoionization pressure, stellar winds, and supernova explosions), is still very uncertain [54]. Together with the thermal structure, interstellar turbulence, and magnetic fields regulate star formation but the relative contribution of the different processes is yet unclear. Galaxy evolution models critically depend on an observational calibration of this kinetic feedback input through observations of the velocity structure within the disturbed volume. Significant momentum impact occurs for regions with densities above 100 cm^{-3} and velocities above a few km/s [38] and this interaction is best traced through [CII] large-scale mapping observations. Measurements of the momentum feedback will enable us to estimate the time scales and physical conditions over which star-formation is suppressed by the removal of molecular material. This is essential in order to evaluate the contribution of starburst galaxies to the global star formation history of the Universe.

2.2 Extragalactic science

The physical conditions in nearby galaxies can be more extreme than those observed in the Milky Way. Even within the Local Group, the massive star cluster R136, powering the 30 Doradus nebula in the Large Magellanic Cloud (LMC), is 10 times more

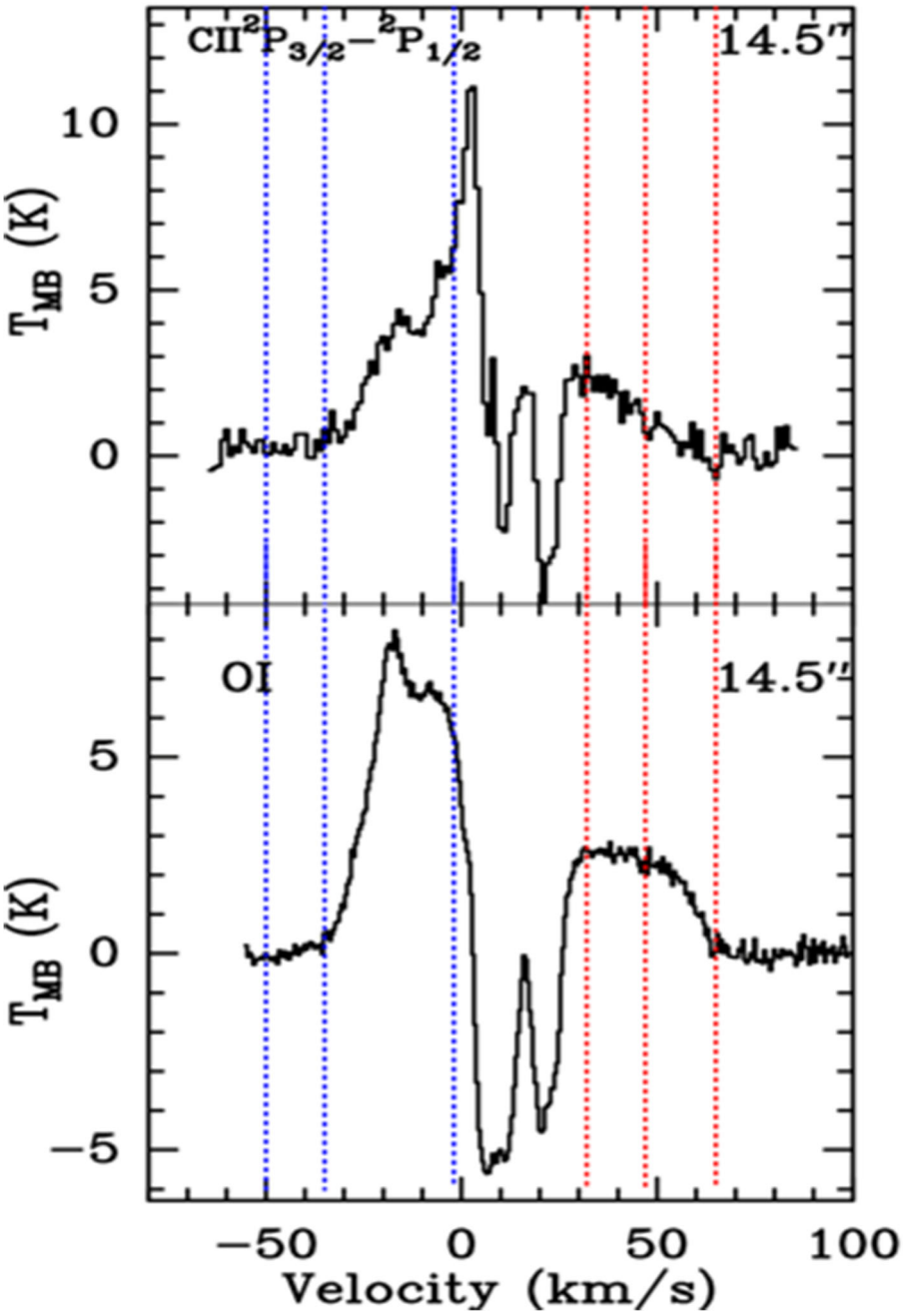

Fig. 5 [CII] and [OI] profiles observed with GREAT/ SOFIA towards the massive star forming region G5.89-0.39 (from [60])

massive than the most massive star cluster in our Galaxy. Beyond the Local Group, extraordinary star clusters in nearby dwarf galaxies (NGC 1569, NGC 1705) are more than 30 times more powerful than R136. To study the vast parameter space spanned by star formation in different environments (nuclei, arms, inter-arms, outer discs) and the detail of different physical and chemical conditions of the ISM (metallicity, mass, density, temperature, velocity, abundances) we need to go beyond the Milky Way and the Local Group of galaxies.

A spectroscopic survey of a volume limited sample of nearby galaxies has the potential to disentangle the contributions of the various ISM phases along the same line of sight, i.e. the contributions from the dense, star-forming molecular gas, photon dominated cloud interfaces, the diffuse molecular and atomic material, and the ionized gas. Such velocity resolved (3-D) observations will shed unprecedented light on the interplay of the ISM phases and their role in the cycle of matter inside galaxies as well as in the evolution of galaxies.

2.2.1 FIR fine-structure lines as probes of star formation activity

With the advent of ALMA, the use of FS lines [CII] 158 μm and [NII] 205 μm as measures of the star formation rate (SFR) is now routinely extended to the high-redshift Universe (the lines shift from the FIR to submillimetre wavelengths). In fact, [CII] detections in redshift z$\sim$6 star-forming galaxies with ALMA are more common than detection of molecular gas e.g., [11, 67, 80, 126].

Yet, the validity of using FIR FS methods to estimate SFR must be fully observationally and theoretically established. The key assumption is the dependence of the dust grain photo-electric heating rate on the specific physical conditions. Models have only been really tested through FIR observations for conditions relevant for dense and intense PDRs such as the Orion Bar [112] and for conditions relevant to diffuse clouds using UV absorption measurements [91]. Nevertheless, Herschel observations of [CII] in the Milky Way show that the [CII]-SFR relation extends over six orders of magnitude, but only by considering that [CII] emission originates from different ISM phases (e.g., dense PDRs, cold HI, CO-dark H_2, and ionized gas: [89]).

As shown in Fig. 4, the [CII]-SFR relation for the combined phases in our Galaxy is consistent with that found for distant galaxies (e.g., [14, 17, 18, 42, 94]). Recent models are also improving our theoretical understanding of this relationship (e.g., [115]). [NII] traces the ionized gas, coming both from the compact HII regions and from the more diffuse component. Herschel observations of our Galaxy (e.g. [48, 85]) show that the [NII] 205 μm line emission is extended and presents broad lines. In distant galaxies, because of its close relation with SFR as a tracer of ionized gas, [NII] is gaining popularity [44, 64, 130]. [CII] 158 μm and [NII] 205 μm, shifted to (sub)mm wavelengths, are observable with ALMA and provide important constraints on the SFR at high z. Indeed, there is some indication that [CII] may not be the best probe because of possible contributions from regions such as dense PDRs and diffuse gas regions that are not directly associated with star formation e.g., [1, 17]. And there may be additional problems; at high FIR luminosities (i.e., high SFR), both [CII] and [NII] are deficient in emission with respect to what would be expected for

a "perfect" (i.e., single power-law) SFR tracer (e.g., [17, 19, 27, 45, 65, 103]). This means that in some regions, and/or over entire galaxies, physical conditions in the ISM are suppressing some of the emission of these lines; warm temperatures, high volume densities, and compact size are possible limiting conditions (e.g., [20]).

Since [CII] and [NII] and other FIR FS lines are the best/brightest line diagnostics of estimates of star-formation activity at high-redshifts, it is crucial to understand the origin of the deficit and develop a better theoretical understanding of the correlation. This can only be done by resolving ISM phases both spatially and kinematically in the Galaxy, the Local Group, and nearby galaxies. Since ALMA can only observe these lines at high redshifts there is a clear need for a facility that will carry out such measurements in the local Universe.

2.2.2 Probing the ISM in external galaxies

It is now well established that galaxies show large variations in the physical and chemical properties of their star forming gas, which regulates their evolution. Existing atomic and molecular observations in a handful of the nearest galaxies, show a chemical diversity and complexity that cannot be explained by a single component, steady-state chemical model, and indicates how relative abundances between atoms and molecules may be able to provide insights into the physical distribution of the gas and the energetics of these galaxies. Observations of the most abundant gas-phase atoms and molecules in nearby galaxies allow us to study the physical characteristics of galaxy environments and measure the amount of gas in each phase of the ISM. A high spectral resolution (heterodyne) instrument will enable us to obtain velocity-resolved maps of the major cooling lines of the ISM in galaxies. High spectral resolution is needed to disentangle the contributions of the various ISM phases along the same line of sight, i.e. the contributions from the dense, star forming molecular gas, photon dominated cloud interfaces, the diffuse molecular and atomic material, and the ionized gas (as shown in Fig. 6).

In Section 2.1.5 we described how [CII] and [NII] have been used to trace the star formation rate both in the Milky Way and beyond. These same arguments apply here to nearby (and distant) galaxies, but without going beyond the Milky Way, the environment and metallicity probed by observations are limited. To truly explore the relation between star-formation activity and its tracers (including CO and dust), it is imperative to examine a wide range of physical conditions in a variety of galaxies.

2.2.3 Line profiles

Line profiles of [CII], [NII], and [OI] reveal the dynamical state of the emitting gas, but can also probe gas accretion and dispersion on global scales, in the nuclei, spiral arms, and the interarm gas, in the metal-rich interiors as well as in metal-poor outskirts. Moreover, it will be possible to study the degree to which unresolved, kinematically correlated structures in the beam contribute to observed line shapes (super-resolution techniques).

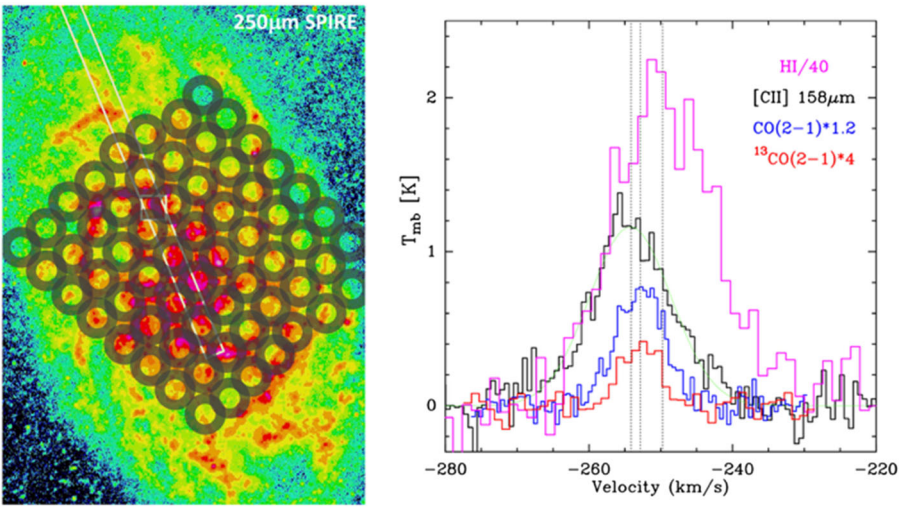

Fig. 6 SPIRE 250 μm image of M33 and PACS spectroscopy of HII regions in M33 in [CII], HI, CO, and ^{13}CO from [51, 73] Grey circles denote the potential spectral imaging FoV with FIRSS

2.2.4 The role of feedback from AGN and massive stars

One of the key Herschel results was the identification of AGN and starburst outflows through the detection of the OH absorption lines (e.g., [108, 109, 117]). The FIRSS Nearby Galaxy Survey (NGS) has the potential to revolutionize the study of the impact of violent events on the surrounding ISM. The kinematics measured by the exquisite spectral resolution of FIRSS will probe the disruption of the ISM through massive star and AGN feedback; in fact, modeling the kinematic information can establish whether the gas is tracing circular motion in a galaxy disc, or non-planar outflows. The potential of this strategy has recently been demonstrated by SOFIA/GREAT observations of spectra of [CII] and [NII] in the nuclear region of the nearby galaxy IC342 [101]. They find that the ionized gas emission shows a kinematic component with the signature of two bipolar lobes of ionized gas expanding out of the galactic plane. Depending on position, 35-90% of the observed [CII] intensity stems from the ionized gas similar to the center of the Milky Way but considerably more than the lower fractions found in less violent regions in the disc (e.g., [89]). Similar studies of the effect of AGN feedback on atomic and fine-structure lines are still in their infancy (e.g., [16, 39]). However, high-velocity HI outflow signatures are common in powerful AGN (e.g., [26, 75]), and inevitably linked to outflows in other tracers including ionized gas (e.g., [61]) and CO (e.g., [13]). Recent observations of [CI] in NGC6240 [12] and NGC 7469 [46] have highlighted the potential of the [CI] line to trace powerful outflows in galaxies. The FIRSS NGS provides a potentially fundamental discovery space for understanding how violence in galaxies impacts the ISM and the consequent changes in the way a galaxy evolves.

2.2.5 Weighing galaxies: The true gas reservoir

The [CII] line is in many cases the brightest cooling line of the ISM in galaxies and its intensity, as has already been discussed, is known to be closely linked to their star formation rate. It probes dense and warm photon dominated regions (PDRs), but also the CO-dark molecular gas, warm and cold atomic clouds, and the diffuse ionised medium. Observations of line integrated intensities at high angular resolutions have been made possible with Herschel/PACS and SOFIA/FIFI-LS. However, disentangling the contributions of the various ISM phases to the [CII] emission is difficult in the absence of velocity information. Herschel/HIFI and SOFIA/GREAT observations of [CII] line profiles have started to shed light on its origin. HIFI observations of [CII] along various lines-of-sight in the Milky Way provided for the first time the necessary velocity resolution to address in particular the importance of the CO-dark molecular gas, the likely precursor of dense molecular clouds that will eventually form stars. These observations have shown that the dominant part of the molecular H_2 gas in the outer parts of the Milky Way is not detected in CO, but in [CII] [88]. These findings agree with high CO-to-H_2 conversion factors found in nearby, low metallicity dwarf galaxies [59, 106]. High spectral resolution FIRSS measurements will, for the first time and in a systematic way, quantify the fraction of CO-dark molecular gas as a function of environment and its impact on the total molecular gas reservoir in galaxies and eventually unveil the true amount of molecular gas in galaxies.

2.3 Distant galaxies

2.3.1 Blind surveys of galaxies (FIR lines)

Understanding how the ISM in galaxies evolves with redshift and luminosity is crucial for determining how galaxies - and star formation within galaxies - evolve, from their birth to the galaxies we observe today in the local Universe. FIR lines, such as [OI], [OIII], [NII], and [CII] are the best tracers of the ISM conditions, also controlling star formation by providing the cooling needed by the clouds to collapse and initiate star formation. The different lines originate in different regions and probe the different physical conditions of the ionized or neutral ISM (i.e., density, ionization potential of the power source, temperature). With the availability of ALMA and NOEMA a surge in detections of the [CII] line from high-z galaxies ($z>3$) has taken place. However, such detections come only from sparse observations of specific targets, each with different characteristics (i.e., redshift, luminosity), and observed at different wavelength, sensitivity, spectral and spatial resolutions. Therefore, a systematic study of the evolution of the ISM in galaxies has, so far, not been possible. FIRSS will provide line observations of unbiased samples of galaxies at different redshifts between $0<z<3$ bridging the local Universe to the high redshift Universe covered by ground facilities (observing in the mm/sub-mm range, where FIR lines are redshifted at $z>3$).

Figure 7 shows an observational setup assuming two bands, centred at [NII] 205 μm and [CI] 370 μm. Using these bands, it will be possible to carry out blind surveys of the [CII] line emitters at $z\sim0.3$ and $z\sim1.35$, of [NII] 122 μm at $z\sim0.7$ and $z\sim2$,

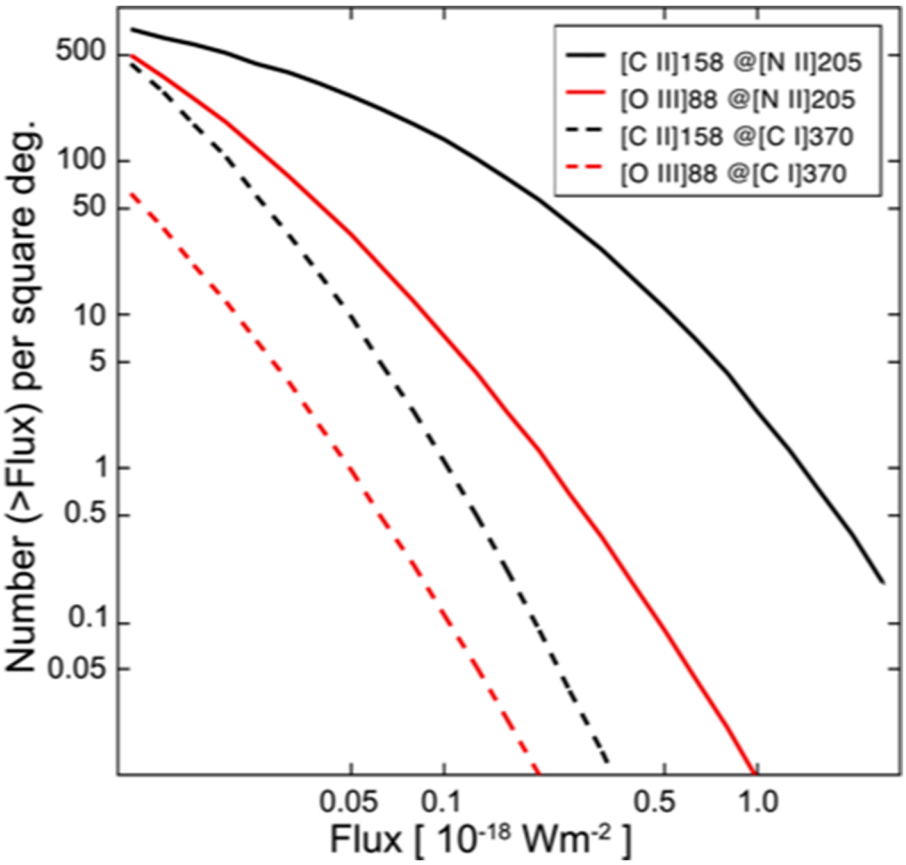

Fig. 7 Number counts expected from FIRSS 'blind surveys' in [NII] 205 μm and [CI] 370 μm channels

of [OIII] 88 μm at z$\sim$1.35 and z$\sim$3.2. Such surveys will enable, for the first time, a statistical study of how lines and the ISM conditions change across different epochs.

2.3.2 Intensity mapping – probing large-scale structure

A deep spectroscopic extragalactic survey at high Galactic latitudes provides an ideal data set for full 3D tomographic intensity mapping of large-scale structure. Such a deep survey is ideal for the detection and physical characterization of line emitting galaxies at various z-intervals, and of rare sources that may also be detectable in several other lines (see Fig. 8).

Beyond individually detected galaxies, above the usual threshold of S/N$\sim$5 for the line flux, the same deep field data can be used to map out the integrated line emission from the galaxies though fluctuations in the integrated emission of spectral lines. Previously, such fluctuation studies (leading to statistical measurement of the ensemble star-forming galaxy properties as well as the cosmic star-formation rate density and cosmic dust abundance) were limited to broadband continuum imaging data. At

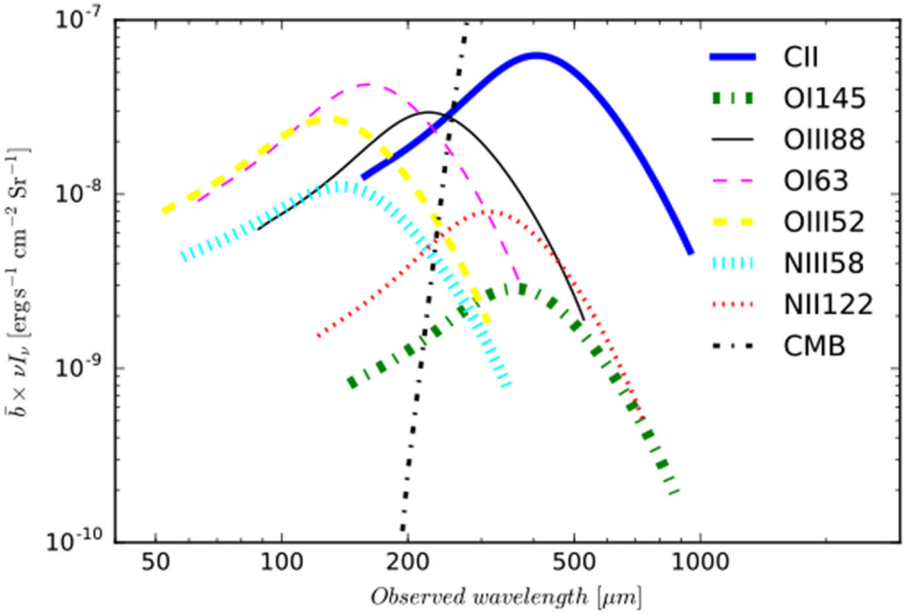

Fig. 8 Intensity of IR fine-structure lines as a function of wavelength. FIRSS would allow observations at 370 μm and 205 μm probing primarily [CII] 158 μm at z=0.3 and 1.3, [OIII] 88 μm at z=1.3, and [OI] 63 μm at z=2.2

FIR/sub-mm wavelengths such studies have been successful with wide surveys of Herschel – SPIRE [3, 110, 119]. However, mapping the statistics of line intensities in a narrow waveband but with significant spectral resolution, increases the value of the data by providing information in the third dimension, permitting an understanding of spectral line emission as a function of redshift. Such a study is similar in spirit to intensity mapping now pursued by the cosmological community using a variety of emission lines as tracers of the large-scale structure. The 21 cm spin-flip line of neutral hydrogen is the most common example, with a variety of low-frequency interferometers pursuing the signal as a probe of reionization. Low-redshift studies have mostly concentrated on rest-frame optical and UV lines, including H_α and Ly_α. FIRSS provides an avenue for intensity mapping in the far-infrared using atomic fine structure lines (e.g. [113]).

3 Science requirements

The science described in the previous sections requires very high spectral resolution observations of 0.3 km/s to 0.03 km/s i.e. R = f/δf of 10^6 to 10^7 to trace the velocity structure of the FIR lines and disentangle the main ISM components along the line of sight. FIRSS will comprise four discrete high spectral resolution receiver channels centred on important FIR fine structure lines. These correspond to target wavelengths (frequencies) of [OI] 63 μm (4.7 THz), [CII] 158 μm (1.9 THz), [NII] 205 μm (1.46

THz) and, [CI] 370 μm (809 GHz). Each receiver band will have an instantaneous bandwidth of 32 GHz in double side band configuration (see discussion in Section 4) and a typical spectral resolution of 5 MHz. The requirements are summarised in Table 1.

4 Key instrument technology

4.1 Achieving the scientific goals

The scientific goals of the Far-Infrared Spectroscopic Surveyor outlined above, require technological solutions that combine high detection sensitivity and high spectral resolving power (resolution order$> 10^6$) within the Terahertz frequency domain. Achieving a spectral resolving power in excess of 10^5 with direct detection systems is very challenging as it implies complex optics, usually gratings, Fourier Transform Spectrometers, and an Etalon. Heterodyne technology, however, provides a viable and attractive solution as heterodyne receivers can easily achieve spectral resolution in excess of 10^6 (or even 10^7, if necessary). Unlike direct detection systems, heterodyne pixel sensitivity is limited by quantum noise and we are already approaching a few times this fundamental limit. This limitation can be overcome with either larger telescopes, or with large arrays of detectors, which can decrease effective integration times by orders of magnitude. To date only single pixel (dual polarization) heterodyne receivers have flown in space. HIFI on board Herschel successfully demonstrated the use of single pixel detectors performing close to the quantum noise limit.

However, single pixel detectors prohibit any large scale mapping. Since the core of the FIRSS science case is to map the entire FIR sky the use of multi-pixel architecture for the heterodyne receivers is an imperative. The proposed instrument configuration is summarised in Table 2. Each of the four FIRSS channels will comprise 128 pixel arrays located in the focal plane of the primary antenna. Each channel will comprise an array of superconducting mixers, a Local Oscillator (LO) chain, stages of intermediate frequency (IF) amplification followed by digital sampling and signal processing. The most sensitive mixers use superconductors and require cooling to $\sim$ 4K. Achieving such low temperatures in space is non-trivial but can be achieved either by flying a reservoir of cryogenic gas (as was done with Herschel) or mechanical cryocoolers.

Table 1 Key science requirements

Science Area	Spectral Resolution km/s	Sensitivity (5σ/1hr) Wm^{-2}	Spatial Resolution arcsec	Min Bandwidth GHz
All-Sky Survey	0.5-1	1×10^{-20}	10-30	10
Galaxies	1-10	1×10^{-21}	10-30	30
Deep Surveys	Not a hard requirement	5×10^{-22}	10-30	32

Table 2 Design parameters for FIRSS receivers

Band	Frequency (THz)	Trx (K)	No of Pixels	Trms (mK)
Band 1	0.81	100	2×64	3.7
Band 2	1.45	200	2×64	5.5
Band 3	1.90	300	2×64	7.3
Band 4	4.7	500	2×64	7.7

Cryocoolers for space have made great advances recently and have been demonstrated by various past missions, e.g. Odin, Planck. A potential configuration would include passively cooling the receivers to 50 K (L2 orbit) and active cooler technology providing sub-stages with necessary heat lift at 15 K and 4 K. The 4 K stage will cool the sensitive mixers and the first stages of low noise amplification. The 15 K and 50 K stages, in addition to reducing the thermal conductive and radiation load on the 4 K stage, also cool the second stage IF amplifiers and can be used to cool the final LO stage to increase its efficiency. The need for multi-pixel systems requires development of processes, procedures, and techniques that can result in robust, repetitive, and cost-effective systems for space telescopes. Besides drastically increasing the pixel count, it is also highly desirable to have broadband RF receivers that provide a considerable increase in science return and only require a modest amount of resources such as mass and power.

The four FIRSS receiver channels will be operating in a double sideband configuration. For Band 1, 2, and 3, conventional multiplier-amplifier chains provide suitable sources of LO power injected into the mixer using a simple beam splitter. For band 4, the LO source is provided by a quantum cascade laser (QCL) cooled to ∼50 K. Each mixer is followed by a cooled low-noise amplifier (LNA) at 4 K, one at the 15 K, and a further stage of ambient temperature amplification, while the IF final output is processed by a dedicated fast Fourier Transform spectrometer (FFTS). Each receiver system is calibrated through the use of two blackbody loads of known brightness temperature that are sequentially introduced into the optical path.

The individual components of the heterodyne receiver are described in more detail below:

4.2 Mixers

The need for state-of-the-art sensitivity defines the use of superconducting mixers, either Superconducting Insolating Superconducting (SIS) mixers or Hot Electron Bolometers (HEB) mixers. SIS mixers, (e.g. [4, 41]), provide near-quantum-noise-limited performance at frequencies up to that of the superconducting band gap, and have demonstrated double-sideband (DSB) sensitivities of ∼2 hf/k. The SIS mixers flown on Herschel are among the lowest noise heterodyne mixers made. Beyond the frequency of about 1.2 THz Hot Electron Bolometers (HEBs) are the most sensitive mixers. Recently, considerable improvements in HEB receiver sensitivity have been made (e.g. [52]). Traditional HEB mixers (Nb-based) are limited to around 3 GHz

intermediate frequency (IF) bandwidth. Published work with novel superconducting materials, such as MgB2, has shown that HEB mixers with an 11-13 GHz IF bandwidth are possible (e.g. [77]) but recent results indicate that IF bandwidths exceeding 20 GHz are also feasible [2]. The large bandwidth is required at THz frequencies to be able to observe lines of $\sim$ 500 km/s width. The FIRSS heterodyne instrument will use HEB mixers for the 1.4 THz, 1.9 THz and 4.7 THz bands aiming to reach sensitivities of about 2 to 3 hf/k. While SIS arrays up to 64 pixels have been demonstrated at low frequencies (300 GHz, [37]), at THz frequencies, 2×7 pixel HEB receivers [96, 97] have been deployed on SOFIA. What is needed for FIRSS is a robust and cost-effective way of producing quantum-limited mixer arrays with 100's of pixels. Integration of mixers with the first stage amplifiers is also important for large arrays.

4.3 Low noise amplifiers

For space missions, the amplifiers not only need to have very low noise, wide bandwidth, and high stability, but also they should have very low power dissipation ($\sim$0.5 mW per IF chain). A gain of about 20 dB is needed for the first cold amplifier, more gain can be added at slightly higher temperatures [93] The amplifiers also need to have a good match to the mixers, or alternatively, isolators need to be developed and inserted between the two. To date, cryogenic SiGe heterojunction bipolar transistor amplifiers have demonstrated the lowest power dissipation (only 0.3 mW) with good noise performance (5K) albeit with an IF bandwidth of 1.8 GHz [71] and 4 GHz [72]. This promising technology therefore requires further development to obtain a wider bandwidth, while keeping the power dissipation low, and a gain of at least 20 dB to avoid the degradation of the front end sensitivity. An alternative, is using the well-established InP technology, which is being employed in numerous ground-based instruments, e.g. the most recent InPs for ALMA [63] and has been space qualified for HIFI/ Herschel (InP cryogenic amplifiers with very good performance are now commercially available [62]). For optimal performance, they typically require around 5 mW of power per amplifier, although operation at reduced power while maintaining good performance has been described [121]. Further experiments are required to investigate their stability and reproducibility at such low power levels. Parametric cryogenic amplifiers are capable of much lower power dissipation with noise performance approaching the quantum limit [25, 120] but they need microwave pumping, which adds complexity. These devices are still to be demonstrated in practical ground-based radio astronomy receivers and are currently at a low TRL level.

4.4 Backend spectrometers

Large format array receivers such as those envisaged for FIRSS require a large number of backends, each operating within an $\sim$8 GHz bandwidth. Traditional approaches such as filter banks, AOS, and Chirp- Transform-Spectrometers (CTS) are bulky and require a substantial amount of DC power (30-40 Watts). FPGA/ASIC-based solutions are currently being developed by European consortiums, while ASIC-based system-on-chip (SoC) architectures are being developed in the US with

the purpose of providing low-power backends for array receivers. A 3 GHz bandwidth CMOS chip based on 65 nm technology has already been demonstrated [47, 129]. This single chip backend can support 4096 channels and requires only 1.65 Watts. To achieve a resolution of 10^6 to 10^7 the 1000 channels need to be configurable to cover more or less IF bandwidth, depending on the observing frequency. This translates into a resolution bandwidth between 4.7 MHz (for [OI] at 0.3 km/s resolution) and 50 kHz (for the 557 GHz water line at 0.03 km/s). We allocate 1W power consumption to each 8 GHz backend. The 4-bit digitization (as used for ALMA) is sufficient. CMOS-based spectrometers are advancing quickly with the telecommunication industry and are predicted to reach the required bandwidth and power within a few years. Current versions have 6 GHz bandwidth, are extremely lightweight (<120 gm), and require little power (< 1W) per backend [49]. An autocorrelation spectrometer (ACS) is another viable option, as it has been used already in space missions (ODIN), balloon mission (TELIS), and low power ASIC versions are becoming available (www.omnisys.se/product/fft-spectrometer/). The goal is to have backend spectrometers that take less than 1 W per band of 8-10 GHz of bandwidth.

4.5 TRL considerations

The FIRSS receivers are based on the successful design of the Herschel/ HIFI instrument. Herschel / HIFI has flown receivers in 7 frequency bands between 480 GHz and 1900 GHz, albeit only one pixel for each of the two polarizations. Simply increasing the number of pixels from 1 to 64 should be possible and will have a TRL of 8. Table 3 summarises the TRL for each component. For the FIRSS instrument, the newest technological developments will be used to keep volume, mass, power, and heat dissipation low. Efficient local oscillators are pumping ~16 mixers at a time. The mixers will need to be packaged into compact arrays with efficient IF extractions. To reduce the LO noise, balanced mixers will be used. The heat dissipation of the cryogenic amplifiers determines the required cooling at 4 K. SiGe amplifiers require 1/10 of the power of the Herschel InP amplifiers, but they have too low bandwidth and are not space qualified, yet. The coolers and the backend spectrometers dominate the overall power budget of the satellite. Low power backends are also essential

Table 3 TRL considerations for FIRS components

Subsystem Description	Current TRL	Heritage
Multiplied LO, f < 2 THz	5	Herschel, MIRO, STO-2 SOFIA, JUICE(SWI)
Multiplied LO, f >2 THz	4	Herschel, STO-2, SOFIA
HEB mixers	4	Herschel, SOFIA, STO-2
SIS mixers	5	Herschel/ HIFI
IF LNAs	4	Herschel/ HIFI
Backend	5	STO-2, SOFIA
Bias electronics	8 / 5	Herschel
Optics	8	Herschel

for FIRSS. CMOS spectrometers use less than 2 W power and are promising candidates for FIRSS. Bias electronics and optics are well established since Herschel, but multiplexing the bias electronics will reduce the heat transfer along cables to the cold front end.

5 Mission profile

5.1 Overview

The FIRSS concept naturally fits into a M-Class mission profile, adopting a profile similar to the ESA M4 Ariel mission [23] with the parameters shown in Table 4. The configuration assumes heterodyne receivers based upon superconducting mixer technology, with superconducting 4 K mixers cooled by closed-cycle cooler technology.

If a smaller, less ambitious, S-Class mission is assumed then the orbit would probably be limited to Low-Earth Orbit (LEO) with a corresponding smaller spacecraft (2m size) with 1m class telescope and spacecraft dry mass $\sim$ 300 kg adopting an ESA S1 CHEOPS [92] mission type profile. Pointing requirements are estimated at an absolute pointing error (APE) of 36 arcsec and relative pointing error (RPE) of 12 arcsec. Such a small class mission would struggle with power / cooling requirements and some of the wavelength channels may have to be correspondingly sacrificed.

5.2 Orbit and survey strategy

The requirement to operate at low temperatures leads to the need for a stable thermal environment. The optimal location for the mission is at the second Earth-Sun Lagrange point (L2). In this location, the gravitational pull of the Sun and the Earth combine, causing the spacecraft to orbit the Sun at the same rate as the Earth, faster than would otherwise occur. This effect allows for a stable thermal environment as well as a relatively short distance to Earth of about 1,500,000 km.

Table 4 FIRSS mission profile

Telescope:	1-2 m class off-axis Cassegrain
Wavelength range:	63 to 370 μm (4.7 THz to 0.81 THz), in 4 bands to match fine structure lines
Dimensions:	$\sim$ 3.6 m
Spacecraft Dry Mass:	$\sim$1000 kg (plus propellant for internal propulsion to L2)
Pointing requirements:	APE: 10″, RPE: $\sim$0.1 pixel at 1 s
Attitude Control System:	classical AOCS architecture, single star tracker, four reaction wheels
Thermal Control System:	Passive cooling via V grooves of telescope to $\sim$50 K, Stirling coolers for 50 K and 15 K
	Joule-Thomson (Planck-like) coolers for 4 K
Orbit:	Lissajous orbit about the Lagrange point L2
Launch:	Launch from Kourou, by an Ariane 62 launch vehicle

With the current single-pixel heterodyne receivers that have flown in space to date, an all-sky map is restrictively time consuming due to the need to ensure appropriate coverage (Nyquist sampled) for each scan line as the detectors move across the sky. Conceptual studies have been carried out and simulations have shown [95], that using single pixel detectors (e.g. a ∼48 arcsec beam for a CI channel), a +/− 5 degree (10 degree strip) survey of the entire Galactic Plane, as shown in Fig. 9, would take approximately 1 year to complete.

Such a survey would cover an area of 3600 sq. deg. or 8% of the sky providing the spectroscopic equivalent of the Herschel imaging HiGAL survey [70]. Note that even with single pixels, such a spectroscopic survey would already provide a quantum leap forwards over any previous spectroscopic survey, e.g. the GOTC^{+} Herschel/HIFI survey that sparse sampled the Galactic plane with 450 lines of sight [88]. At the time of the Voyage 2050 programme as discussed in Section 4, we would expect multi-pixel arrays to be viable thus allowing full sky coverage, including naturally deep coverage at the ecliptic poles.

5.3 Configuration

The configuration of the spacecraft will be similar to that of Planck. The spacecraft will consist of three main components as shown in Fig. 10: the Service Module (SM), the thermal shields, and the Payload Module (PM). To realise the science goals, a 1-2 metre class off-axis Cassegrain is assumed. The proposed configuration allows the spacecraft to yaw away from the Sun vector by up to 50° before the payload is directly illuminated, significantly more than the required value of 8°. Tighter constraints are placed on the yaw by the location of the radiators, although this can be optimised

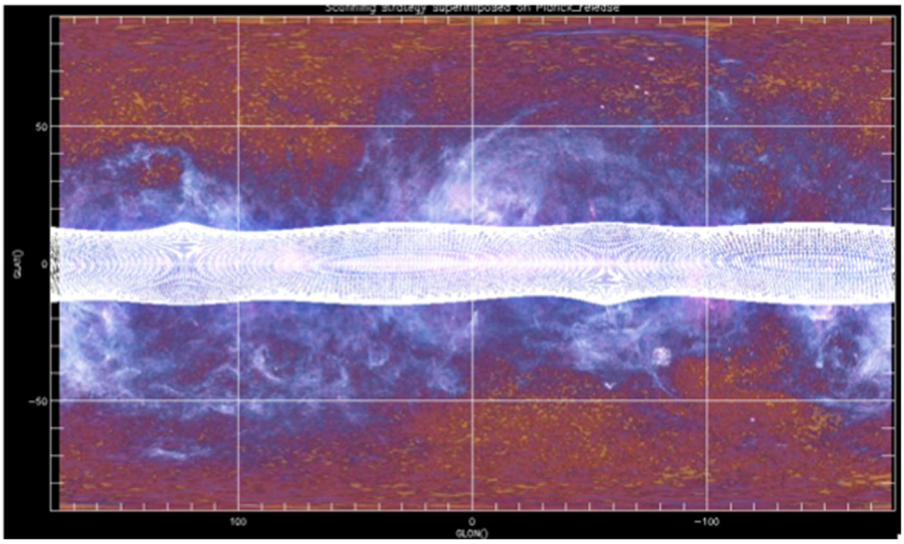

Fig. 9 Simulated survey strategy of the Galactic Plane (+/-5 degrees) assuming single pixel detectors, scan lines (in white) overlaid on the Planck map

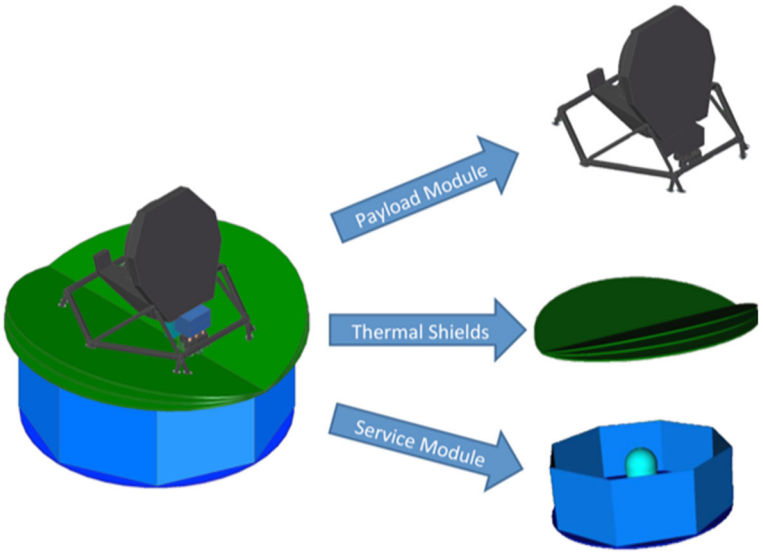

Fig. 10 FIRSS Spacecraft Configuration (credit: the FIRSPEX team)

during study phases as has been done in the past for similar spacecraft designs such as that of Ariel [23].

The overall thermal control design concept is driven by the need for the instruments to operate at ∼4 K. The low temperature required at instrument level is achievable by placing the spacecraft at L2 and through a combination of passive cooling, use of high reflective surfaces, in conjunction with active cooling of the instrument focal plane by means of dedicated cryo-coolers (Stirling and Joule-Thomson) and has been previously studied for missions such as Planck, Ariel, and SPICA. The payload module design is based on a horizontal telescope orientation. The receiver payload unit is located below the telescope near to the axis of the V-grooves thermal shields, thus being close to the Service Module to minimize the length of the thermal couplings to the cryo-cooler cold-heads.

5.4 Launcher

Together with the mission orbit, the cryogenic requirements of the mission will influence the spacecraft configuration in two ways: First, the use of multiple cryo-coolers for achieving the required sensitivities, has led to a large power demand from the payload. This has, in turn, resulted in the use of a large solar array as well as a large structure to accommodate the required radiators for heat rejection. Second, in order to keep the payload at cryogenic temperatures, a large sunshield is necessary. Through its V-groove design, the thermal shield both passively cools the payload and protects it from direct solar illumination. The thermal shield is also required to protect the payload from dissipations from the spacecraft, hence resulting in a structure with a size slightly larger than the Service Module structure. FIRSS could be launched by

an Ariane 62 from Kourou and injected into a direct transfer trajectory to L2 lasting approximately 30 days. Following this, FIRSS will be commissioned and then start its science observing plan.

5.5 FIRSS in the international astronomy context

The widely-appreciated importance of fine structure lines has been emphasized by the results from Herschel and new results emerging from ALMA. For Galactic studies, a large-scale survey of [CII] was carried out at high spectral resolution with the HIFI instrument [34]. However, as eludicated above, this survey only sampled a few hundred points spaced approximately every degree in longitude, and did not result in images of any [CII]-emitting region. Only one giant molecular cloud, Orion, was even partially imaged [32, 81]. Indeed, only $\sim$0.06% was covered by HIFI heterodyne spectroscopy. GREAT on SOFIA has allowed limited observations of [CII] and [NII] and the upGREAT receiver having 14 mixers has improved on mapping speed and added the [OI] capability. Nevertheless, with only on the order of 100 hours per year available for any one instrument, and an estimated 20 years to cover the Galactic plane, it is clear that the required scientific objectives cannot be achieved on SOFIA. Similarly, for balloon based experiments such as STO2 (e.g. [123]) and GUSTO [5], given the flight durations (weeks), smaller apertures and limited channels (GUSTO will not observe CI), it will not be possible to carry out the wide area, multi-channel surveys required for the science objectives expressed in this proposal. Although there are future space borne facilities with impressive capabilities for far-infrared – submillimetre spectroscopy such as SPICA [100] and the Origins Space Telescope [8], both of these facilities are classed as observatories, dedicated to detailed spectroscopic observations of a limited number of sources. FIRSS is the only mission that will provide velocity-resolved information for large areas of our Galaxy and nearby galaxies. The FIRSS concept is a surveyor mission and instead will provide the spectroscopic equivalent to the wide-field to all-sky imaging surveys afforded by IRAS, AKARI and Herschel.

Acknowledgements Part of this research was carried out at the Jet Propulsion Laboratory, California Institute of Technology, under a contract with the National Aeronautics and Space Administration.

Declarations

Conflict of Interests The authors declare that they have no conflict of interest.

References

1. Abdullah, A., et al.: ApJ **842**, 4 (2017)
2. Acharya, N., Novoselov, E., Cherednichenko, S.: MgB2 HEB terahertz mixers: Diffusion- or phonon-cooled? Submitt IEEE T Thz Sci Techn (2019)
3. Amblard, A., Cooray, A., Serra, P., et al.: Nature **470**, 510 (2011)
4. Baryshev, A.M., et al.: A&A **577**, 129 (2015)
5. Bernasconi, P., Walker, C., Kulesa, C.: The GUSTO balloon mission. Cospar **42**, 304 (2018)
6. Bisbas, T.G., Tanaka, K.E.I., Tan, J.C., Wu, B., Nakamura, F.: ApJ **850**, 23 (2017)
7. Boggess, N.W., Mather, J.C., Weiss, R., et al.: ApJ **397**, 420 (1992)
8. Bradford, M.C., et al.: The Origins Survey Spectrometer (OSS): a far-IR discovery machine for the Origins Space Telescope. SPIE **10698**, 18 (2018)
9. Bregman, J.N.: In: The Interplay Between Massive Star Formation, the ISM and Galaxy Evolution (1996)
10. Brunt, C.M., Heyer, M.H., Mac Low, M.-M.: In: Kunth, D., Guiderdoni, B., Heydari-Malayeri, M., Thuan, T.X. (eds.) A&A, 504, 883, p. 211 (2009)
11. Capak, P.L., Carilli, C., Jones, G.: Nature **522**, 455 (2015)
12. Cicone, C., Severgnini, P., Papadopoulos, P.P., et al.: ApJ **863**, 143 (2018)
13. Cicone, C., Maiolino, R., Sturm, E., et al.: A&A **562**, 61 (2014)
14. Cigan, P., Young, L., Cormier, D.: AJ **151**, 14 (2016)
15. Dame, T.M., Hartmann, D., Thaddeus, P., et al.: ApJ **547**, 792 (2001)
16. Debuhr, J., Zhang, B., Anderson, M., et al.: arXiv:1512200386 (2014)
17. de Looze, I., Fritz, J., Baes, M., et al.: A&A **571**, 69 (2014)
18. de Looze, I., Baes, M., Bendo, G.J., Cortese, L., Fritz, J.: MNRAS **416**, 2712 (2011)
19. Diaz-Santos, T., et al.: ApJ **774**, 68 (2013)
20. Diaz-Santos, T., et al.: ApJ **846**, 32 (2017)
21. Dobbs, C.L., et al.: In: Beuther, H., H, R.S., Klessen, C.P. (eds.) Protostars and Planets VI (2014)
22. Draine, B.: ApJ **732**, 100 (2011)
23. Eccleston, P., et al.: An integrated payload design for the Atmospheric Remote-sensing Infrared Exoplanet Large-survey (ARIEL). SPIE **9904**, 33 (2016)
24. Elmegreen, B.G., Parravano, A.: ApJ **435**, 121 (1994)
25. Eom, B.H., et al.: Nat. Phys. **8.8**, 623 (2012)
26. Fabian, A.C., Wilkins, D.R., Miller, M.J., et al.: MNRAS **424**, 217 (2012)
27. Farrah, D., Lebouteiller, V., Spoon, H.W., et al.: ApJ **776**, 38 (2013)
28. Fixsen, D.J., Bennet, C.L., Mather, J.C.: ApJ **526**, 207 (1999)
29. Franeck, A., Walsch, S., Glover, S.C., et al.: In: Simon, R., Schaaf, R., Stutzki. J. (eds.) Conditions and impact of star formation. EAS Publications Series (2016)
30. Franeck, A., Walch, S., Seifried, D., et al.: MNRAS **481**, 4277 (2018)
31. Girichidis, P., Naab, T., Walch, S., et al.: ApJL **816**, 17 (2016)
32. Goicoechea, J.R., Teyssier, D., Etxaluze, M., et al.: ApJ **812**, 75 (2015)
33. Goldbaum, N., Krumholtz, M.R., Matzner, R., et al.: ApJ **738**, 101 (2011)
34. Goldsmith, P., Yildiz, U., Langer, W.D., et al.: ApJ **814**, 133 (2015)
35. Grenier, I.A., Casandjian, J.-M., Terrier, R.: Science **307**, 1292 (2005)
36. Grenier, I.A., Black, J.H., Strong, A.W.: ARA&A **53**, 199 (2015)
37. Groppi, C., Walker, C., Hungerford, A., Kulesa, A., et al.: 345-GHz array receiver for the Heinrich Hertz Telescope. ASP Conference Proceedings **217**, 48–49 (2000)
38. Haid, S., Walch, S., Seifried, D., et al.: MNRAS **478**, 4799 (2018)
39. Hamer, S.L., Edge, A.C., Swinbank, A.M., et al.: MNRAS **437**, 826 (2014)
40. Herbstmeier, U., Kerp, J., Snowden, S.L., Mebold, U.: A&A **272**, 514 (1993)
41. Hedden, A., Tong, E., Blundell, R., Papa, D.C., Smith, M., Honingh, C.E., Jacobs, K., Pütz, P., Wulff, S., Chang, S., Hwang, Y.: Upgrading the SMA 600 GHz receivers. Proc. ISSTT 428–432 (2010)
42. Herrera-Camus, R., Bollato, A., Wolfire, M., et al.: ApJ **800**, 1 (2015)
43. Heyer, M., Krawczyk, C., Duval, J., Jackson, J.M.: ApJ **699**, 1092 (2009)
44. Hughes, T.M., et al.: A&A **587**, 45 (2016)
45. Ibar, E., et al.: MNRAS **449**, 2498 (2015)
46. Izumi, T., Nguyen, D.D., Imanishi, M., et al.: ApJ In Press (2020)
47. Kim, Y., Zhang, Y., Tang, A., Reck, T., Chang, M.-C.F.: A 183-GHz InP/CMOS-hybrid heterodyne-spectrometer for spaceborne atmospheric remote sensing. International symposium for space terahertz technology (2018)

48. Kirk, H., et al.: ApJ **723**, 457 (2010)
49. Klein, B., Hochgürtel, S., Krämer, I., Bell, A., Güsten, R.: A&A **542**, L3 (2012)
50. Klessen, R.S., Hennebelle, P.: A&A **520**, 17 (2010)
51. Kramer, C., et al.: Star Formation in M33 (HerM33es). EAS Publications Series **52**(2011), 107 (2011)
52. Krause, S., Meledin, D., Desmaris, V., Belitsky, V.: IEEE Trans. Terahertz Sci. Technol. **8**(3), 365–371 (2018)
53. Kruijssen, J.N.M.D., Longmore, S.N., Elmegreen, B.G.: MNRAS **440**, 3370 (2014)
54. Krumholz, M.R., Bate, M.R., Arce, H.G., et al.: In: Beuther, H., Klessen, R.S., Dullemond C.P., Henning, T. (eds.) Protostars and Planets VI, pp. 243–266 (2014)
55. Lada, C.J., Lombardi, M., Roman-Zuniga, C.: ApJ **778**, 133 (2013)
56. Langer, W.D.: ASP Conference Series **417**, 71 (2009)
57. Langer, W.D., Velusamy, T., Pineda, J.L., et al.: A&A **521**, L17 (2010)
58. Langer, W.D., Velusamy, T., Pineda, J.L., et al.: A&A **561**, A122 (2014)
59. Leroy, A., Bolatto, A., Gordon, K., et al.: ApJ. **737** 12 (2011)
60. Leurini, S., Wyrowski, F., Wiesemeyer, H.: A&A **584**, 70 (2015)
61. Liu, G., et al.: MNRAS **436**, 2576 (2013)
62. Lopez-Fernandez, I., Gallego, J.D., Diez, D., Barcia, A.: Wideband ultra-low noise cryogenic InP IF amplifiers for the Herschel mission radiometers. IEEE MTT-S Int. Microwave Symp. Dig. 1907–1910 2006 (2006)
63. López-Fernández, I., Gallego, J.D., Diez, C., Barcia, A., Pintado, J.M.: Development of cryogenic IF low-noise 4-12 GHz amplifiers for ALMA radio astronomy receivers. SPIE **4855**, 489–500 (2006)
64. Lu, N., et al.: ApJ **802**, 1 (2015)
65. Luhman, M.L., et al.: **504** 11 (1998)
66. Lutz, D.: ARA&A **52**, 373 (2014)
67. Maiolino, R., et al.: MNRAS **452**, 54 (2015)
68. Miville-Deschenes, M.-A., Duc, P.-A., Marleau, F., et al.: A&A **593**, 4 (2016)
69. Molinari, S., Swinyard, B.M., Barlow, M., et al.: A&A **518**, 100 (2010)
70. Molinari, S., et al.: A&A **591**, 149 (2016)
71. Montazeri, S., Wong, W.T., Coskun, A., Bardin, J.C.: A wide-band high-gain compact SIS receiver utilizing a 300 micronW SiGe IF LNA. IEEE Trans. Microwave Theor. Techniq. **64**(1), 178–187 (2016)
72. Montazeri, S., Grimes, P., Tong, C.E., Bardin, J.C.: ITTST **6**(1), 133–140 (2016)
73. Mookerjea, B., et al.: A&A **532**, 152 (2011)
74. Mookerjea, B., Israel, F., Kramer, C., et al.: A&A **586**, 37 (2016)
75. Morganti, R., Tadhunter, C.N., Osterloo, T.A., et al.: A&A **444**, 9 (2005)
76. Nishimura, Y., Shimonishi, T., Watanabe, Y., et al.: ASPC **499**, 165 (2015)
77. Novoselov, E., Cherednichenko, E.: Gain and noise in THz MgB2 Hot-Electron Bolometer Mixers with a 30-K critical temperature. IEEE Trans. Terahertz Sci. Technol. **7**(26), 704–710 (2017)
78. Oliver, S., et al.: MNRAS **424**, 1614 (2012)
79. Ossenkopf, V., Koumpia, E., Okada, Y.: A&A **580**, 83 (2015)
80. Ota, K., Fabian, W., ohta, K.: ApJ **792**, 34 (2014)
81. Pabst, C., Higgins, R., Goicoechea, J.R., et al.: Nature **565**, 618 (2019)
82. Park, S.-J., Min, K.-W., Seon, K.-I., et al.: ApJ **700**, 155 (2009)
83. Peretto, N., Andre, P., Könvyes, V., et al.: A&A **541**, 63 (2012)
84. Perez-Beaupuits, J.P., et al.: A&A **575**, 9 (2015)
85. Persson, C.M., Gerin, M., Mookerjea, B., et al.: A&A **568**, 37 (2014)
86. Pilleri, P., Fuente, A., Gerin, M., et al.: A&A **561**, A69 (2014)
87. Pineda, J.R., Velusamy, T., Langer, W.D., et al.: A&A **521**, 19 (2010)
88. Pineda, J.L., Langer, W.D., Velusamy, T., Goldsmith, P.F.: A&A **554**, 103 (2013)
89. Pineda, J.L., Langer, W.D., Goldsmith, P.F.: A&A **570**, 121 (2014)
90. Planck Collaboration XIII, Planck Collaboration: A&A **571**, 13 (2014)
91. Pottasch, S.R., Wesselius, P.R., van Duinen, R.J.: A&A **74**, 15 (1979)
92. Rando, N., et al.: CHEOPS: the characterizing exoplanets satellite ready for launch. SPIE **10698**, 14 (2018)
93. Ravindran, P., Chang, S.-W., Gupta, D., Inamdar, S., et al.: IEEE Trans. Appl. Superconductiv. **3**, 25 (2015)
94. Rigopoulou, D., Hopwood, R., Magdis, G.E., et al.: ApJL **781**, 15 (2014)

95. Rigopoulou, D., et al.: The Far-Infrared Spectroscopic Explorer (FIRSPEX): probing the lifecycle of the ISM in the Universe. SPIE **9904**, 2 (2016)
96. Risacher, C., Güsten, R., Stutzki, J., Hübers, H.-W., et al.: First supra-Thz heterodyne array receivers for astronomy with the SOFIA observatory. IEEE Trans. Terahertz Sci. Technol. **6**, 199–211 (2016a)
97. Risacher, C., Güsten, R., Stutzki, J., Hübers, H.-W., et al.: A&A **595**, 34 (2016)
98. Roberts, W.W.: ApJ **158**, 123 (1969)
99. Roberts, W.W.: ApJ **173**, 249 (1972)
100. Roelfsema, P.R., et al.: PASA **35**, 30 (2018)
101. Roellig, M., Simon, R., Gusten, R., et al.: A&A **519**, 33 (2016)
102. Roy, N., Frank, S., Carilli, C.L., et al.: ApJ **834**, 171 (2017)
103. Sargsyan, L., et al.: ApJ **755**, 171 (2012)
104. Schneider, N., Gusten, R., Tremblin, P., et al.: A&A **542**, 18 (2012)
105. Schneider, N., Csengeri, T., Bontemps, S., et al.: A&A **520**, 49 (2010)
106. Schruba, A., Leroy, A., Walter, F., et al.: AJ **143**, 138 (2012)
107. Smith, R.J., Glover, S., Clark, P.C., Klessen, R.S., Springel, V.: MNRAS **441**, 1628 (2014)
108. Spoon, H.W.W., Farrah, D., Lebouteiller, V., et al.: ApJ **775**, 127 (2013)
109. Sturm, E., Gonzalez-Alfonso, E., Veilleux, S., et al.: ApJ **733**, 16 (2011)
110. Thacker, C., Gong, Y., Cooray, A., et al.: ApJ **811**, 125 (2015)
111. Tang, N., Li, D., Heiles, C., et al.: A&A **593**, 42 (2016)
112. Tielens, A.G.G.M., Meixner, M.M., van der Werf, P.P.: Science **262**, 86 (1993)
113. Uzgil, B., Aguirre, J.E., Bradford, M., et al.: ApJ **793**, 116 (2014)
114. Vallee, J.P.: ApJ **681**, 303 (2008)
115. Vallini, L., Gallerani, S., Ferrara, A.: ApJ **813**, 36 (2015)
116. Vazquez-Semadeni, E.: Magnetic fields in diffuse media, Astrophysics and Space Science Library **407**, 401 (2015)
117. Veilleux, S., Melendez, M., Sturm, E., et al.: ApJ **776**, 27 (2013)
118. Velusamy, T., Langer, W.D., Goldsmith, P.F., et al.: A&A **578**, 135 (2015)
119. Viero, M.P., Moncelsi, L., Quadri, P., et al.: ApJ **779**, 32 (2013)
120. Vissers, M.R., et al.: Low noise kinetic inductance traveling-wave amplifier using three-wave mxing. Appl. Phys. Lett. **1**(01), 108 (2016)
121. Wadefalk, N., et al.: Cryogenic wide-band ultra-low-noise IF amplifiers operating at ultra-low DC power. IEEE Trans. Microwave Theor. Techniq. **51.6**, 1705–1711 (2003)
122. Wakker, B.P., van Woerden, H.: ARA&A **35**, 217 (1997)
123. Walker, C., et al.: SPIE **7733**, 0 (2010)
124. Wang, P., Li, Z.-Y., Abel, T., et al.: ApJ **709**, 27 (2010)
125. Wiesemeyer, H., Güsten, R., Heyminck, S., et al.: A&A **585**, 76 (2016)
126. Willott, C.J., Carilli, C., Wagg, J., Wang, R.: ApJ **807**, 180 (2015)
127. Wolfire, M.G., McKee, C.F., Hollenbach, D., Tielens, A.G.G.M.: ApJ **587**, 278 (2003)
128. Xu, D., Li, D., Yue, N.: ApJ **819**, 22 (2016)
129. Zhang, Y., Kim, A., Tang, J., Kawamura, T.R., Chang, M.C.F.: A 2.6 gs/s spectrometer system in 65nm cmos for spaceborne telescopic sensing. In: IEEE International Symposium On Circuits and Systems (ISCAS), Florence, Italy, pp. 1–4 (2018). https://doi.org/10.1109/ISCAS.2018.8351690
130. Zhao, Y., Lu, N., Xu, K., et al.: ApJ **820**, 118 (2016)

Affiliations

D. Rigopoulou[1] · C. Pearson[2] · B. Ellison[2] · M. Wiedner[3] · V. Ossenkopf Okada[4] · B. K. Tan[1] · I. Garcia-Bernete[1] · M. Gerin[3] · G. Yassin[1] · E. Caux[5] · S. Molinari[6] · J. R. Goicoechea[7] · G. Savini[8] · L. K. Hunt[9] · D. C. Lis[10] · P. F. Goldsmith[10] · S. Aalto[11] · G. Magdis[12] · C. Kramer[13]

1 Astrophysics, Department of Physics, University of Oxford, Keble Road, Oxford, OX1 3RH, United Kingdom

2 RAL Space, Science Technology Facilities Council, Harwell Campus, Didcot, OX11 0QX United Kingdom

3 LERMA, Observatoire de Paris, PSL Research University, CNRS, Sorbonne Universités, UPMC, Univ. Paris 06, F-75014, Paris, France

4 Physikalisches Institut, Universität zu Köln, Zuelpicher Str. 77, 50937 Köln, Germany

5 Institut de Recherche en Astrophysique et Planétologie (IRAP formerly CESR), BP 44346, 31028, Toulouse Cedex 4, France

6 INAF-Istituto di Astrofisica e Planetologia Spaziale, via Fosso del Cavaliere 100, 00133, Roma, Italy

7 Grupo de Astrofisica Molecular, Instituto de Ciencia de Materiales de Madrid (CSIC), E-28049, Madrid, Spain

8 Department of Physics and Astronomy, University College London, Gower St., London, WC1E 6BT, United Kingdom

9 Osservatorio Astrofisico di Arcetri, Florence, Italy

10 Jet Propulsion Laboratory, California Institute of Technology, 4800 Oak Grove Drive, Pasadena, CA 91109, USA

11 Department of Space, Earth and Environment, Onsala Space Ob- servatory, Chalmers University of Technology, SE-439 92 Onsala, Sweden

12 DTU-Space, Technical University of Denmark, Elektrovej 327, DK-2800 Kgs., Lyngby, Denmark

13 Institut de Radioastronomie Millimétrique (IRAM), 300 rue de la Piscine, 38406 Saint Martin d' Hères, France